RSC Advances

ROYAL SOCIETY OF CHEMISTRY

www.rsc.org/advances

Investigation of Templated and Supported Polyaniline Adsorbent Materials

M. H. Mohamed[1]; A. Dolatkhah[1]; T. Aboumourad[1]; L. Dehabadi[1]; and L. D. Wilson[1*]

[1]Department of Chemistry, University of Saskatchewan, 110 Science Place, Saskatoon, Saskatchewan, S7N 5C9

***Corresponding Author**: L. D. Wilson, Tel. +1-306-966-2961, Fax. +1-306-966-4730, Email: lee.wilson@usask.ca

Abstract

Various structural forms of poly(aniline) (PANI) were synthesized in aqueous solution with different acids and/or a chitosan template support to afford nanoparticle PANI (**NP**; synthesized in water), bulk-PANI (aqueous acetic acid (**HAc**), hydrochloric acid (**HCl**) and sulfuric acid (**SA**) and a chitosan-PANI composite (**CH**) material. The polymer materials were characterized using spectroscopy (^{1}H NMR, FT-IR, UV-vis), TGA and P-XRD. The polymer materials were structurally diverse according to their unique morphology related to the ratio between quinoid and benzenoid monomer units of PANI. The sorption and kinetic uptake properties of PANI materials with methylene blue (MB) in aqueous solution were studied where variable sorption capacity was observed, as follows: **NP** > **HAc** > **HCl** > **SA** > **CH**. The Sips isotherm model describes the adsorptive equilibrium uptake while the pseudo-second order kinetic model describes the time dependent uptake of MB. The monolayer sorption capacities (Q_m) reported herein are among the highest (*ca*. 6-fold greater) relative to other Q_m values reported for PANI materials in the literature.

Keywords: polyaniline; chitosan; methylene blue; adsorption; isotherm

Introduction

The use and uncontrolled release of organic and inorganic dyes into aquatic environments is a consequence of various industrial processes. Discharge of dyes through wastewater release to the environment adversely affect ground and surface water environments, and both human and ecosystem health.[1-2] Methylene blue (MB) is a widely used industrial textile dye and there have been many approaches to sequestration of MB from industrial wastewater that differ by their efficiency, cost and environmental impact.[3-4] The aromatic structure of MB contributes to its relative stability and recalcitrant nature; thus, a range of removal methods have been investigated that include oxidation[5], catalytic degradation[6], electrocatalytic[7-8], thermocatalytic[9], photocatalytic[10] and adsorption[11]. Adsorption is a practical removal method for waterborne organics because of its general versatility, facile operation, relatively low cost, and energy efficiency.[1-2, 7, 12-13]

Several common adsorbents such as alumina, silica gel, zeolites, activated carbon (AC), and biomaterial adsorbents have been used for the removal of dyes.[1-2, 14-15] In the case of AC, it exists in various structural forms suitable for the purification of air and various pollutants from industrial wastewaters; powdered (PAC), granulated (GAC), pellet (ACP), and fiber (ACF).[14, 16-19] In part, this is due to its highly porous structure and surface area of AC,[20] in agreement with the variable uptake toward MB (21.5 - 980 mg/g).[11, 21-23] However, the relative material and regeneration costs of AC are high and the attenuation of it sorptive efficiency after recycling limits its wider applicability for specialized remediation problems.[24-25]

Polyaniline (PANI) is a unique adsorbent material because of its relatively low cost, facile synthesis, chemical stability, and tunable properties.[26] Structural tunability of

PANI is evidenced by the formation of hybrid polymers with different morphologies (e.g.,ribbons[27], dendritic[28], fibers and wires[29], and sheets[30]). Synthetic modification of PANI is related to its unique protolytic behaviour (*cf*. Scheme 1),[31] as evidenced by the imine nitrogen sites of the emeraldine base (EB) and emeraldine salt (ES) forms of PANI. ES is an acid-base complex between a nitrogen group and a base which affords a composite or doped PANI material.[32] PANI materials are used in rechargeable batteries, solar cells, sensors, anti-static and anti-corrosion coatings, asymmetric films, and membranes.[33] PANI sorbent materials have been used for the uptake of sulfonated dyes[34] and Direct Blue 78 from water.[35] Conventional PANI, PANI nanoparticles (PANI-NPs) and PANI nanotubes (PANI-NTs) and its composites were reported to adsorb MB and malachite green.[4, 36-38] The sorptive uptake properties of PANI-based adsorbents are often limited by their limited surface area; however, modified materials such as PANI-NPs and/or composites may display improved properties.[4, 36, 39]

Herein, we report the synthesis and characterization of different structural types of PANI at variable conditions (i.e. acid strength, dilution, and polymer template). The uptake properties of PANI materials at equilibrium and kinetic conditions were investigated using methylene blue (MB).[4, 27, 28]

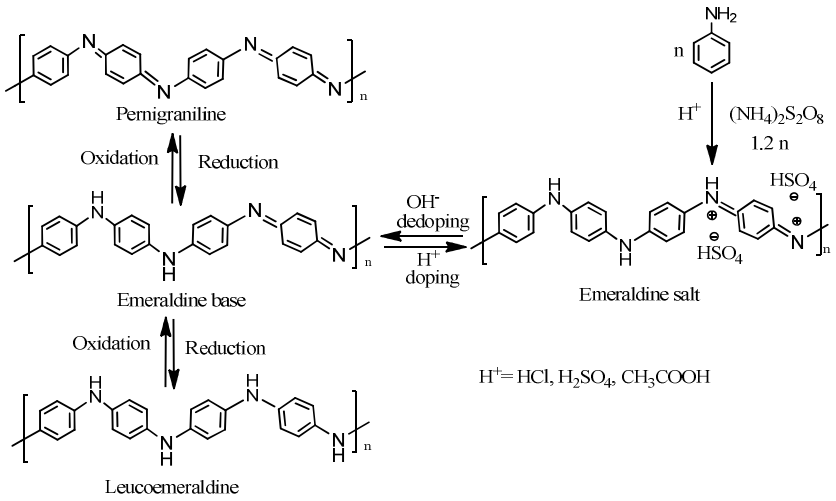

Scheme 1. Illustration of the synthesis, chemical structure, acid/base doping/de-doping chemistry of polyaniline/sulfuric acid and ammonium sulfate by-products.

Materials and methods

Materials

Aniline (99.5% pure), acetic acid, methylene blue (MB), chitosan (low molecular weight, 75-85% deacetylated), dimethyl sulfoxide (DMSO) and semi-permeable dialysis tubing were purchased from Sigma-Aldrich Canada Ltd. Ammonium peroxydisulfate (APS, 98.0% pure), ammonia, hydrochloric acid and sulfuric acid were obtained from Alfa Aesar, BDH, Fisher scientific and EMD USA respectively. Dialysis tubing closures purchased from the Spectra/Por company. All chemicals were used as received without further purification unless stated otherwise.

Synthesis of water-catalyzed PANI

PANI nanoparticles (nano-PANI; **NP**) were synthesized by adding of 0.978 ml aniline (0.0107 mol) in 200 mL of Millipore water with stirring for a period of 30 min. Separately, 2.94 g APS (0.0129 mol) was added to 200 mL of Millipore water with a molar ratio of 1.2:1 relative to aniline. The diluted products were mixed for 30 min. with subsequent addition of APS into the aniline solution. The resulting solution was stirred for 24 h. The products were washed with excess Millipore water, vacuum filtered, and dried for 24 h at room temperature. The dried PANI product was deprotonated with excess 0.1 M ammonia. The product obtained was 0.740 g and [74.2% yield].

Synthesis of acid-catalyzed PANI

PANI in bulk solution (bulk-PANI) was synthesized similarly as the NP; however the aniline and APS were likewise diluted 10-fold in 20 mL of 0.1 M of HCl. The other PANI polymers were prepared by substituting 20 mL of HCl with 20mL of 0.1 M acetic acid and 0.1 M sulfuric acid. The weight of bulk-PANI products and the yields (%) were as follows: (**HCl**): 0.922 g [92.5%], acetic acid (**HAc**): 0.951g [95.4%], sulfuric acid (**HS**): 1.315 g [82.7%].

Synthesis of composite PANI

Chitosan (0.2 g) was dissolved in 20 ml of 0.1M HCl for 1 h until a clear solution was obtained. Separately, 0.365 ml of aniline dissolved in 20 ml of 0.1M HCl was stirred for 1 h and allowed to equilibrate for 24 h. After 24 h, a solution of 1.2:1 APS to aniline

(1.095 g) in 20 mL of 0.1 M HCl was added to the mixture and left to mix for 1 h. The addition of the APS solution to the chitosan/aniline solution was followed by an additional hour of mixing. The combined solutions were mixed for 24 h and then washed with excess Millipore water and vacuum filtration, followed by drying for 24 h at ambient conditions. The product (**CH**) was deprotonated with 0.1 M ammonia until a neutral pH was achieved where the weight and yield was 0.623 g [31.2%].

Preparation of MB solutions

MB with the molecular formula $C_{16}H_{18}N_3ClS$ (formula weight = 319.85 g/mol) was used as the dye adsorbate in this study. MB displays a maximum wavelength of absorbance at approximately 663 nm. A calibration curve was created in order to determine the molar absorptivity at λ = 663 nm to establish the working range of concentrations. A 10 mM MB stock solution was prepared by dissolving 1.5 g of MB in 0.5 L of Millipore water (0.3% w/w) with appropriate dilution in water of the stock MB solution to achieve the required concentration as determined by the Beer-Lambert law.

Characterization of polymers

Thermograms of the polymers were obtained using thermogravimetric analysis, TGA (Q500 TA Instruments). Samples were heated in open platinum pans at 25 ºC and allowed to equilibrate for 5 min prior to heating at a scan rate of 5 ºC/min up to 900 ºC. FT-IR spectra were obtained with a Bio-RAD FTS-40 spectrophotometer where samples were analyzed as powders in reflectance mode. Solid samples were prepared by co-grinding polymers (about 5 mg) with pure spectroscopic grade KBr (50 mg) in a small mortar and pestle. The DRIFT (Diffuse Reflectance Infrared Fourier Transform) spectra

were obtained at 295 K with a resolution of 4 cm^{-1} over the 400–4000 cm^{-1} region. DRIFT spectra were recorded with multiple scans in reflectance mode and corrected relative to spectroscopic grade KBr. The intensity of the DRIFT spectra is reported in Kubelka–Munk units. ^{1}H-NMR was done with a wide-bore (89 mm) 11.7 T Oxford superconducting magnet system equipped with 5 mm PATX1 probe operating at 500 MHz. Operating parameters were controlled using a SSSC 500 console and workstation running X-WIN NMR 3.5 (Bruker Bio Spin Corp; Billerica, MA, USA). The Top Spin 1.3 software included the various standard pulse programs for collection of all NMR spectra. A Varian Cary 100 Scan UV–vis spectrophotometer was used to measure MB absorbance (λ_{max} = 663 nm) spectra in aqueous solution and to analyze electronic transitions of the PANI materials dissolved in DMSO. Structural properties of the PANI materials were studied using powder X-ray diffraction (P-XRD). Diffractograms were collected using PANalytical Empyrean powder X-ray diffractometer using monochromatic Co-Kα1 radiation. The applied voltage and current were set to 40 kV and 45 mA, respectively. The samples were mounted in a horizontal configuration after evaporation of hexane films. The PXRD patterns were measured in continuous mode over a 2θ range of 6-45^{o} with a scan rate of 3.2^{o}/min.

Adsorption isotherms and modeling

Fixed amounts (~ 10 mg) of the powdered and sieved polymer materials were mixed with 3 mL of aqueous solution containing different amounts of aqueous dye (0.1–1.5 mM) after equilibration on a horizontal shaker (SCILOGEX SK-O330-Pro) for 24 h. The initial (C_o) and final (C_e) values for MB solutions were determined by measuring absorbance at 663 nm by using UV-vis absorption spectroscopy. The sorption isotherms

are depicted as plots of the adsorbed amount of MB in the polymer phase per mass of sorbent (Q_e; mmol/g) versus the residual equilibrium concentration of MB (C_e). The value of Q_e is defined by eqn 1 where C_o is the initial MB concentration, V is the volume of solution, and m is the mass of sorbent.

$$Q_e = \frac{(C_o - C_e) \times V}{m} \qquad (1)$$

The sorption isotherms were fitted using Langmuir [40], Freundlich [41] and Sips [42] isotherm models (*cf*. Eqns 2-4). The Langmuir model assumes that the adsorbent surface is homogeneous, while the Freundlich and Sips models account for surface heterogeneities. The binding constant is represented by an equilibrium parameter (K_i). The sum of square of errors (SSE) was used as a criterion of the "best fit" while a lower SSE value (*cf*. Eqn 5) indicates an overall greater goodness-of-fit. The optimal fit was obtained by minimizing the SSE for all data across the range of conditions investigated. Q_{ei} is the experimental value, Q_{ef} is the fitted value, and N is the number of Q_e data points.

$$Q_e = \frac{K_L Q_m C_e}{1 + K_L C_e} \qquad (2)$$

$$Q_e = K_F C_e^{1/n_f} \qquad (3)$$

$$Q_e = \frac{Q_m (K_S C_e)^{n_s}}{1 + (K_S C_e)^{n_s}} \qquad (4)$$

$$SSE = \sqrt{\frac{(Q_{ei} - Q_{ef})^2}{N}} \qquad (5)$$

Adsorption kinetics and modeling

Relative kinetic uptake experiments were performed using an *in-situ* one pot set-up. Briefly, a length of the dialysis tubing (6 cm) was cut to size and soaked in the aqueous MB solution for ~ 2 h. One end of the tubing was clipped using the weighted closures. 10 mg of each respective PANI material was added and the opposite end was closed. The tubing housed with the powdered copolymer was immersed in a 120 mL MB solution. 3.00 mL of the dye was pipetted out at variable time intervals and quantified using UV-Vis spectroscopy at λ_{max}=664 nm without further dilution. The data was fit using a pseudo-first order (PFO)[43] and pseudo-second order (PSO)[44] model, as described by Eqn (6-7), respectively. Q_t and Q_e are the amount of dye adsorbed at any time (t) and at equilibrium, respectively. k_i is a rate constant (k_1; $i = 1$) for PFO and k_2 (where $i = 2$) for the PSO, and t is the time. Similar to the equilibrium isotherms, the SSE (*cf.* Eqn 5) was used as a criterion of the "best fit" between theory and experiment.

$$Q_t = Q_e(1 - e^{-k_1 t}) \qquad (6)$$

$$Q_t = \frac{Q_e^{\,2} k_2 t}{1 + k_2 t Q_e} \qquad (7)$$

Results and Discussion

The DRIFT spectra were normalized in order to compare the relative differences between the respective PANI materials. Fig. 1 shows the IR region of interest (2000-500 cm^{-1}) where the quinoid (**Q**) ring stretching is often observed at 1590 and 1586 cm^{-1} for strong and weak acids, respectively.[45] In this work (*cf.* Table 1), a blue shift of the C-C skeletal modes is observed with increased acidity, in agreement with a previous report.[45] The benzenoid (**B**) ring stretching band occurs at 1507 cm^{-1} for strong acids; whereas, a band appears at 1505 cm^{-1} for weak acids such as water.[45] Similar blue shifts were

observed in Table 1. The presence of both **B** and **Q** signatures support the conclusion by Kaplan et al. where the PANI-EB form consists of alternating benzenoid diamine and quinoid diimine units.[46] The ratio of peak areas for **Q** ring stretching relative to that for **B** decreases with increased acidity, as follows: 1.21 (NP), 1.19 (AC), 1.17 (HC), and 1.10 (HS). This infers that the amount of **Q** rings relative to **B** ring units vary with acid strength. In all cases, the observed C=C stretching of aromatic rings and N=N stretching occurred ~1446 cm^{-1} for all the PANI materials except for the chitosan supported PANI. However, the band intensity becomes attenuated with increased acidity. The phenazine ring stretching is seen at 1414 cm^{-1} for the PANI materials except for NP observed at 1416 cm^{-1}. The C-N stretching vibration band is observed ~1375 cm^{-1} (C-N stretching in the neighborhood of a **Q** ring)[47] for all PANI materials except NP. The C-N band overlaps with the band centered at ~1300 cm^{-1}. The integrated peak area increases with greater acid strength: **HAc** (4.65), **HCl** (4.88) and **HS** (4.92), while the peak ~1041 cm^{-1} (present in all materials except for the PANI composite) is attributed to the HSO_4^-/SO_3^- group on sulfonated aromatic ring systems.[48] This band is attenuated with increased acidity, as evidenced by the relative peak areas: **NP** (4.30), **HAc** (3.77), **HCl** (3.53), and **HS** (3.28). The bands near 831-691 cm^{-1} are attributed to substituted ring systems where the cumulative peaks areas are as follows: **HA**c (11.9), **HCl** (12.8), **HS** (11.9) and **NP** (14.7). The IR results indicate that **NP** has more phenazine-like structures relative to bulk PANI.

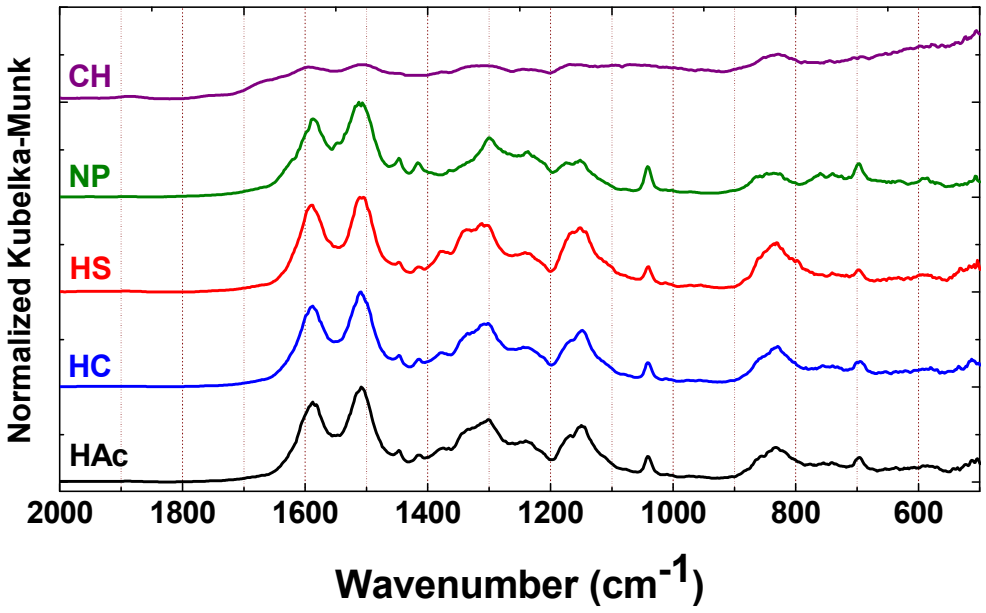

Fig. 1. Normalized FTIR spectra of the PANI materials.

Table 1 FT-IR bands in the 2000-500 cm^{-1} region for the main absorption bands of each PANI material.

Wavenumber (cm^{-1})					Assignment
HAc	**HCl**	**HS**	**NP**	**CH**	
1587.6	1587.8	1588.5	1587.5	1594.1	Quinoid (Q) ring stretching
1508.4	1509.3	1511.1	1513.0	1504.9	Benzenoid (B) ring stretching
1446.6	1446.6	1447.0	1446.5	-	C=C stretching of aromatic ring / N=N stretching
1414.8	1414.7	1414.6	1416.1	1415.0	Phenazine ring-stretching
1375.2	1376.2	1375.5	-	1378.0	C-N stretching in QBQ units
1301.6	1308.3	1311.9	1300.0	1314.1	ν(C-N) of secondary aromatic amine
1240.6	1237.8	1241.9	1236.8	1246.3	ν(C-N) BBB unit
1167.1	1176.9	1180.7	1175.0	1168.0	N=Q=N/δ(C-H)
1150.0	1148.3	1151.7	1151.7	1155.2	B-NH-B/δ(C-H)
1041.2	1041.1	1040.5	1041.4	-	$HSO4^-/SO3^-$ group on sulfonated aromatic ring
856.04	858.53	862.39	858.11	851.54	γ(C-H) (1,2,4-trisubstituted ring) / B ring deformation
831.91	829.49	830.78	836.89	827.55	γ(C-H) (1,4-disubstituted ring) / Q ring deformation
740.76	756.27	740.83	760.42	744.46	γ(C-H) (mono- vs 1,2-disubstituted ring)
695.66	694.57	697.66	697.20	691.10	*Out-of-plane* ring bending (mono-substitution)

Fig. 2 shows the ^1H NMR spectra for the PANI materials in the low field region (δ = 9.5 - 5.5 ppm), where δ = 9.35, 9.30 and 9.08 ppm are assigned to the intermolecular H-bond *via* the carbonyl group.[49-50] The chemical shift ~ 8.6 ppm is assigned to amine proton while the signals at δ = 9.5 - 8.6 ppm disappear when D_2O is added to **NP** (*cf.* Fig.

2). The aromatic protons are observed downfield at δ = 7.93-6.99 ppm. The spectral region between 6.26-5.50 ppm is assigned to protons from the hetero-junction structural regions.[50] Specifically, the protons near δ = 6.2 and 5.7 ppm are attributed to the presence of substituted 1,4-*p*-benzoquinones.[49] **CH** shows a single broad resonance between 7.25-6.75 ppm indicating the aromatic ring system of PANI.

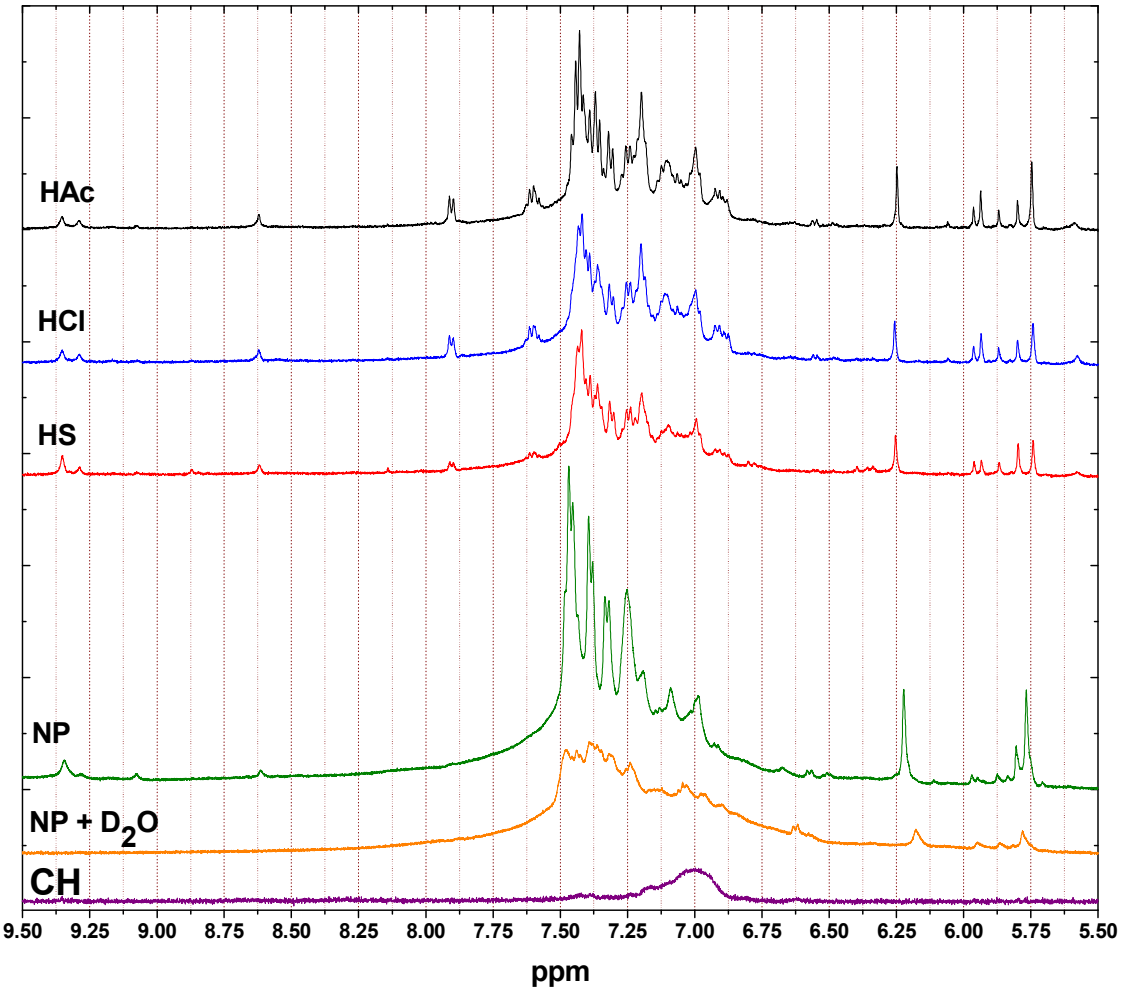

Fig. 2. ^{1}H NMR spectra recorded at 295 K and 500 MHz in DMSO-d_6. Chemical shifts are reference to TMS (δ = 0.0 ppm).

First derivative TGA plots are shown in Fig. 3 and the accompanying thermal parameters are listed in Table 2. There are four thermal events with weight loss profiles were observed for the PANI materials across the temperature range. The first thermal event (*cf*. Table 2) is attributed to desorption of water since PANI is known to be hygroscopic.[51] Since the TGA experiments were conducted in an open pan environment where surface dehydration occurs below 100^{o}C. Maximum water loss appears at different temperatures for all the materials. **NP** has the lowest intensity peak for maximum water loss followed by bulk-PANI and subsequently the composite material. Table 1 illustrates similar trends for the other PANI materials for the loss of water. The second thermal event for **NP** has a lower maximum decomposition temperature; $T_{max\text{-}d}$ (300 ^{o}C) compared to the bulk-PANI, a follows: 322 (**HAc)**, 323 (**HCl**) and 341 ^{o}C (**HS**). This result agrees with a previous report inferring that **NP** has more oligomer components relative to the bulk-PANI because of its more granular in morphology.[48] Results from the weight loss profiles show that **NP** reveals a higher weight loss (24.6%) compared to the bulk-PANI as follows: 14.0% (**HAc**), 14.1% (**HCl**), and 9.42% (**HS**). As the acid strength increases, the PANI materials become more globular in nature. TGA evidence of such structural features is observed from the third thermal event where a similar trend is shown for the $T_{max\text{-}d}$, % weight loss and peak area (*cf*. Table 2). The peak area ratio of the third and the second thermal events are as follows: 2.00 (**HAc**), 2.00 (**HCl**), 3.17 (**HS**) and 0.764 (**NP**). The relative peak areas provide support that **NP** morphology is more linear in nature whereas **HS** is more globular in nature. It is noteworthy that the second thermal event has low temperature shoulders for each of the PANI materials indicates that decomposition is a heterogeneous process. The fourth thermal event in the high

temperature regime is similar for all of the materials (T_{max-d} ~750 ^{o}C). As well, the ratio of weight loss (%) for the latter thermal event relative to the sum of the second and third thermal events are as follows: 0.210 (**HAc**), 0.232 (**HCl**), 0.248 (**HS**), and 0.216 (**NP**). The TGA for **CH** is different from the other materials in terms of the thermal events (2 and 3) with the former representing decomposition of chitosan and the latter is attributed to PANI. TGA results for pure chitosan (not shown) show a single thermal event with a T_{max-d} at 295^{o}C with a 48.1 % weight loss. By comparison, **CH** reveals two thermal events that provide additional evidence for the presence of PANI in the composite material.

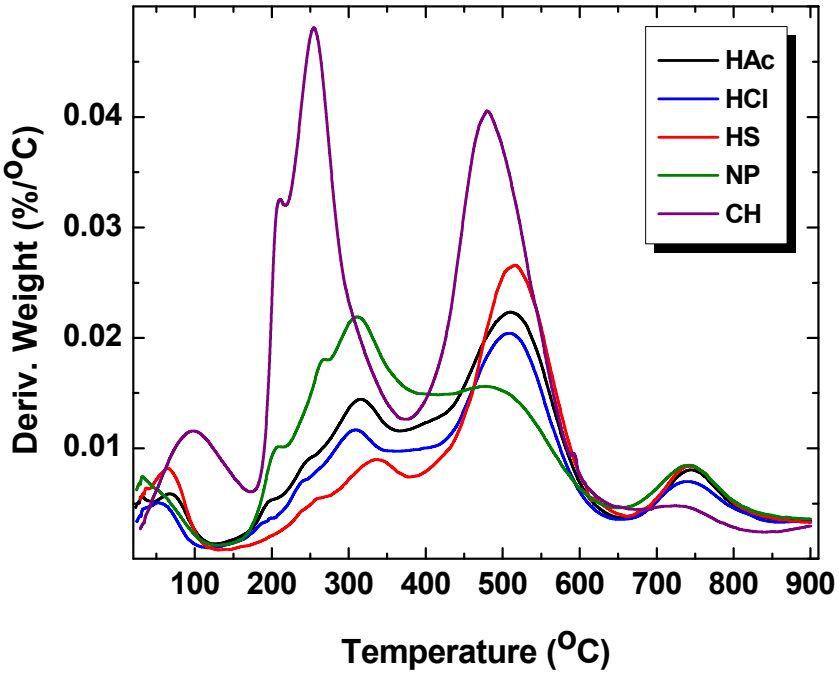

Fig. 3. First derivative TGA plots (weight loss/^{o}C *vs* temperature) of PANI materials.

Table 2. Temperature range, weight loss (%),T_{max-d} (^{o}C) and peak area (%·min/^{o}C) for the four (**1-4**) thermal events (*cf*. Fig. 3) of the various PANI materials

Material	Parameters	Thermal Events			
		1	**2**	**3**	**4**
HAc	**Temp. range (^{o}C)**	25.0-126	126-366	366-652	652-900
	Weight Loss (%)	2.98	14.0	28.0	8.84
	T_{max-d} (^{o}C)	53.6	322	507	749
	Peak area (%·min/^{o}C)	0.192	1.92	2.74	0.600
HCl	**Temp. range (^{o}C)**	25.0-117	117-375	375-651	651-900
	Weight Loss (%)	2.50	14.1	27.9	9.75
	T_{max-d} (^{o}C)	50.5	323	509	753
	Peak area (%·min/^{o}C)	0.269	2.00	2.52	1.12
HS	**Temp. range (^{o}C)**	25.0-134	134-381	381-661	661-900
	Weight Loss (%)	3.75	9.42	29.9	9.74
	T_{max-d} (^{o}C)	58.9	341	518	752
	Peak area (%·min/^{o}C)	0.567	1.79	3.04	1.57
NP	**Temp. range (^{o}C)**	25-131	131-407	407-648	648-900
	Weight Loss (%)	2.81	24.6	18.8	9.36
	T_{max-d} (^{o}C)	38.2	300	487	751
	Peak area (%·min/^{o}C)	0.538	3.25	2.73	1.36
CH	**Temp. range (^{o}C)**	25.0-177	177-376	376-666	666-900
	Weight Loss (%)	5.01	21.1	23.5	3.29

	T_{max-d} (^oC)	99.2	254	485	880
	Peak area (%·min/^oC)	0.255	3.59	4.00	0.0524

P-XRD for PANI materials (*cf.* Fig. 4) show similar spectra except for **CH** which is highly amorphous in nature. The diffraction lines of the other PANI materials are less sharp (more amorphous) with increasing acid strength. This supports the TGA evidence that PANI materials prepared with strong acid afford more granular morphology while water catalyzed PANI (**NP**) affords linear (oligomers) PANI. Linear PANI enables more efficient packing and long-range order which is further evidenced by the distinctive strong and sharp peak observed at $2\theta = 7.61^o$. The diffraction results indicate the presence of oligomers and phenazine-like units.[52] Moreover, the signatures indicate the organization of the PANI chains into nanotubes or lamellae.[48, 53-54] As shown in Fig. 4, the intensity of the peak decreases in the following order: **NP** > **HAc** > **HCl** > **HS**. Additional diffraction peaks are observed (upon magnification of the P-XRD) for the NP materials are denoted by the following lines: $2\theta = 21.9^o$, 23.3^o, 27.3^o, 30.3^o, 31.3^o, 33.4^o and 34.2^o. The other PANI materials show reduced scattering due to band broadening. Interestingly, **HS** has two broad peaks (not observed in the other materials) at $2\theta = 11.0^o$ and 17.8^o. PANI-EB has been reported to have a single broad peak[55-57] or several other P-XRD peaks[54, 58] between from $2\theta = 15\text{-}35^o$. In this work, the PANI-EB materials prepared herein are more crystalline as evidenced by the appearance of several distinctive peaks. These results support the idea that the acid-catalyzed PANI adopts a more granular morphology which increases as the acid strength increases for the PANI synthesis. On the

other hand, **NP** has a more linear morphology, according to the synthetic conditions, as evidenced by the presence of linear oligomers.

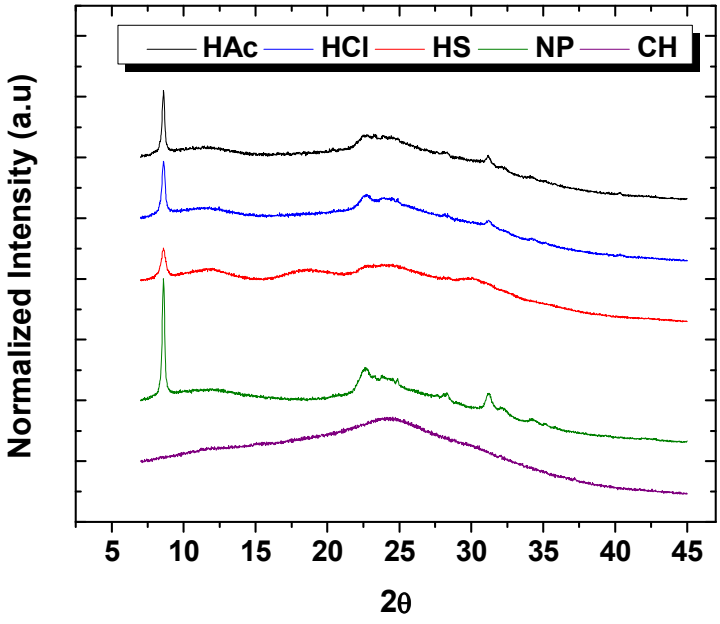

Fig. 4. Powder X-ray diffraction spectra of PANI materials at 295 K.

Fig. 5 shows the UV-vis spectra of the PANI materials. The de-doped form of PANI exhibit two absorption maxima at ~ 320-326 nm and 598-620 nm represents the π-π* transition of the benzenoid ring and n-π* transition between the HOMO of the benzenoid ring (N nonbonding electrons) and the LUMO (π*) of the quinoid ring, respectively.[59-62] In this work, the UV-vis absorption maxima vary for each material (**HAc** and **NP**) where two absorption maxima are seen in the region between 250-400 nm. The λ_{max} for **HAc** is 296 nm and 341 nm and the bands for **NP** are observed at 283 and 358 nm. The other PANI materials display a signature with a λ_{max} in the same region

(333 nm for **HCl** and **HS;** 329 nm for **CH**). In the 500-800 nm region, **NP** is the only material that displays two bands (peak deconvolution using Origin Lab 8); 592 and 621 nm. The other materials display λ_{max} at the following values: 624 (**HAc**), 627 (**HCl**), 624 (**HS**) and 649 nm (**CH**). The latter region is associated with the n-π* transition which tends to have an increased intensity from **NP** to bulk-PANI (with increasing acid strength) and composite PANI has the highest intensity. This infers that the number of benzenoid diamine units increase relative to quinoid diimine units which lead to an increased electronic transition between the two types of materials. This observation is supported by the IR results as discussed above on the peak ratios of **Q** relative to **B**.

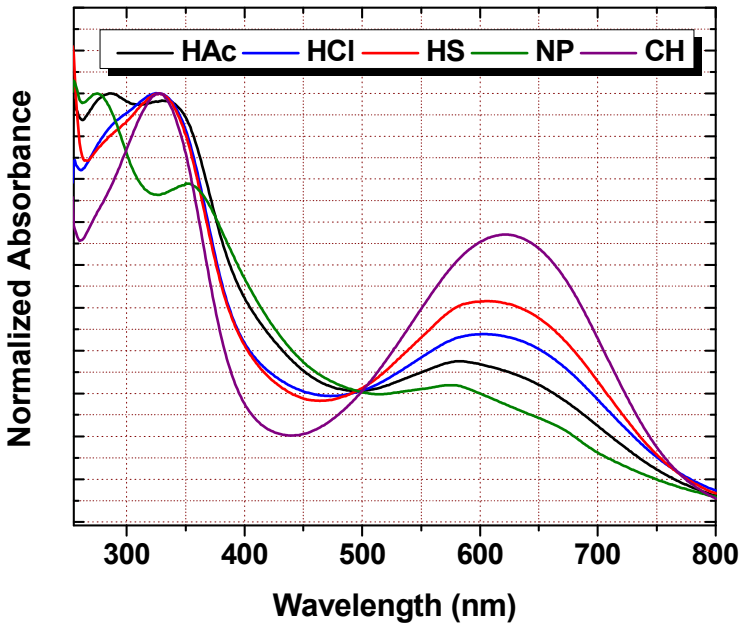

Fig. 5. UV-Vis spectra for the PANI materials in DMSO solution.

The isotherm results for the sorption of MB by the various PANI materials (i.e. **HAc**, **HCl**, **HS**, **NP** and **CH)** are shown in Fig. 6. The value of Q_e increases nonlinearly

as the total concentration of MB increases, reaching monolayer saturation conditions at higher values of C_e. The relative magnitude of Q_e varies according the solvent system used for the synthesis of the PANI materials. The Sips model provides the "best-fit" the three models employed (*cf*. Eqn 2-4), as evidenced by the minimized SSE values by Eqn 5. In the case of **NP**, the uptake of MB increases markedly at low C_e values, achieving saturation of the adsorption sites near 0.2 mM. The other PANI materials reveal a gradual increase of Q_e as C_e increases, attaining a monolayer surface coverage (Q_m ~ 0.7 mM). The Q_m value (parentheses; mmol/g) obtained from the Sips isotherm model decreases in the following order: **NP** (0.267) > **HAc** (0.139) > **HCl** (0.109) > **HS** (0.0813) > **CH** (0.0624). This trend indicates that PANI materials prepared in dilute acid display greater Q_m values. Moreover, the chitosan supported material had the lowest uptake of MB. The binding affinity (K_s; mM^{-1})can be derived from the Sips isotherm parameter (K_s) where the units are given in parentheses in descending order: **NP** (27.6) > **HS** (2.60) > **HCl** (1.68) > **CH** (1.37) > **HAc** (1.33). **NP** has the highest sorption affinity, which correlates with its greater sorption capacity. However, there is no correlation between Q_m and K_s for the bulk-PANI and composite material, as reflected by the heterogeneity parameter (n_s; eqn 4). Bulk-PANI prepared with strong acids has greater sorption affinity despite its lower sorption capacity. This suggests that the morphology affects the sorptive affinity of MB towards the PANI materials. The sorptive uptake capacities of MB obtained herein are significantly greater than other reported studies of PANI or its supported materials reported in the literature (*cf*. Table 3).

Table 3. Comparison of the monolayer sorption capacities (Q_m) of MB with various PANI and supported materials from the literature and this study

Sorbent Material	Sorption capacity (mg/g)	Reference	Solvent System
PANI-EB-NTs/ silica composite	10.3	[36]	0.1 M acetic acid
PANI-EB-NTs	9.21	[4]	0.5 M acetic acid
PANI-EB	13.9	[37]	0.1 M hydrochloric acid
PANI-EB	11.5	[38]	32% hydrochloric acid
NP	85.4	This work	Water
HAc	44.5		0.1 M acetic acid
HCl	34.9		0.1 M hydrochloric acid
HS	26.0		0.1 M sulphuric acid
CH	20.0		0.1 M hydrochloric acid

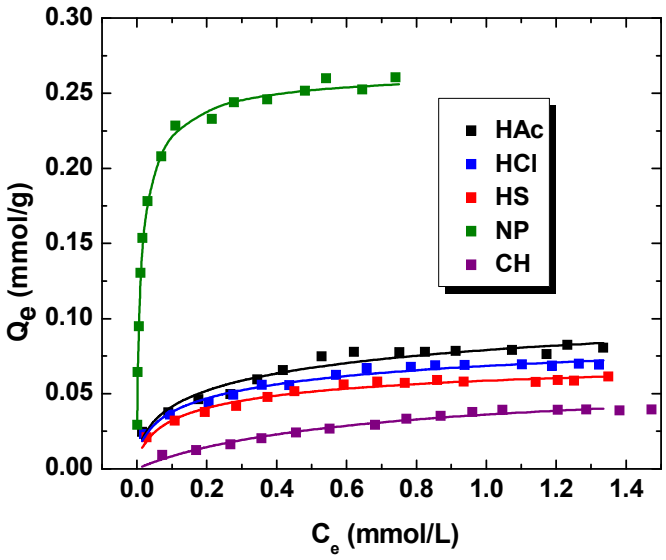

Fig. 6. Adsorption isotherms of MB by PANI materials at pH 7.00 and 295 K.

Fig. 7 illustrates the time dependent sorptive uptake of MB with the various PANI materials. The kinetic uptake of MB varies significantly between **NP**, bulk-PANI, or the **CH** composite material. The time dependent uptake for each system is well described by

the PFO model (*cf*. Eqn 6),as evidenced by the "best-fit" in Fig. 7. The value of Q_e given in parentheses (μmol/g) for the various PANI materials: **NP** (39.6), **HAc** (23.4), **HCl** (22.7), **HS** (22.8) and **CH** (15.4). As expected, kinetic uptake shows a similar to the trend observed for the isotherm adsorption studies. Similarly, the value of k_1 (parentheses; min^{-1}) are as follows: **NP** (0.0171), **HAc** (0.0206), **HCl** (0.0254), **HS** (0.0371) and **CH** (0.0445). The trend for the k_1 values are opposite to that shown for Q_e. This effect may be related to the fractional coverage, θ (Q_e/Q_m) where the θ values increase in the following order: **NP** (0.148) < **HAc** (0.168) < **HCl** (0.208) < **CH** (0.247) < **HS** (0.280).

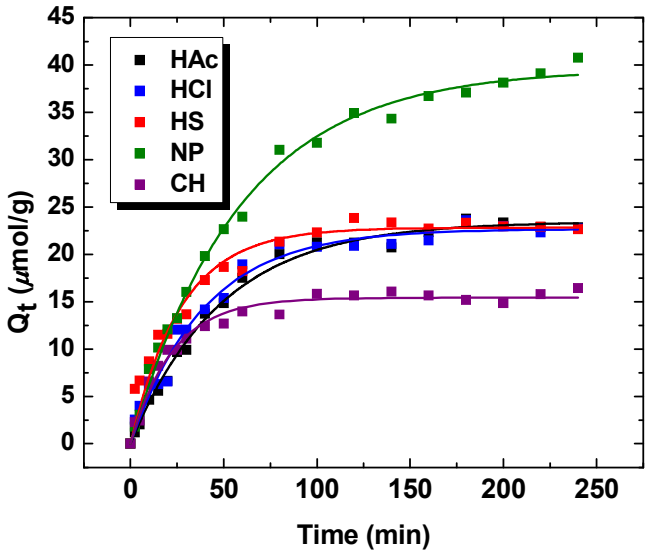

Fig. 7. Kinetic uptake studies of MB with the PANI materials at pH 7.00 and 295 K.

Conclusions

A series of water insoluble PANI nanomaterials and a chitosan supported polymer were prepared using acid catalyzed reactions. Variable yields (31% to 95%) and characterization methods (^{1}H NMR and DRIFT spectroscopy) provided strong evidence

for the PANI materials. The use of different acids and chitosan afforded PANI materials with variable structure due to changes in the relative proportion of PANI containing benzenoid vs. quinoid rings. Quinoid rings are generally formed with increasing acid strength, as evidenced by the electronic transitions (n-π* transition between the HOMO of the benzenoid ring and the LUMO of the quinoid ring), according to the UV-vis spectroscopy results. IR spectroscopy indicates the presence of phenazine-like structures for all the materials, especially NP because it has greater content when compared with bulk-PANI. TGA results indicate that the morphology of the various PANI materials differ from **NP** because it has greater levels of oligomers whilst bulk-PANI possesses a granular morphology. The incorporation of PANI onto chitosan supports is confirmed by P-XRD and TGA. The equilibrium and kinetic uptake properties of the PANI materials vary considerably between **NP,** bulk-PANIs, and **CH. NP** shows the greatest uptake of MB (6-fold greater Q_m) compared to related materials reported (*cf*. Table 3) to date. Thus, the synthetic strategy reported herein affords materials with enhanced uptake properties; however, the rate processes are attenuated with reduced fractional coverage. In the case of **NP**, it has the lowest rate of uptake and this may be due to competitive hydration arising from intraparticle diffusion which arises from differences between bulk and nanoparticle systems. This work has contributed to the development of PANI with diverse structural forms (NP, bulk, and CH supported materials). Further studies are underway to further examine the structure-function relationship of such materials with regard to their adsorption properties. We anticipate that the controlled synthesis of PANI in diverse structural forms will contribute to the development of unique materials for

diverse applications that includes optical sensors and molecular wires for electrochemical devices, among others.[63,64]

Acknowledgements

The authors are grateful to the University of Saskatchewan for supporting this research. MHM acknowledges the MITACS Accelerate Program and Nanostruck Technologies Inc. for PDF funding for this research.

References

1. M. T. Yagub, T. K. Sen, S. Afroze and H. M. Ang, *Adv. Colloid Interface Sci.*, 2014.
2. M. A. M. Salleh, D. K. Mahmoud, W. A. W. A. Karim and A. Idris, *Desalination*, 2011, 280, 1-13.
3. P. Sharma, N. Hussain, D. J. Borah and M. R. Das, *J. Chem. Eng. Data*, 2013, 58, 3477-3488.
4. M. M. Ayad and A. A. El-Nasr, *J. Phys. Chem. C.*, 2010, 114, 14377-14383.
5. H. Sun, S. Liu, S. Liu and S. Wang, *Applied Catalysis B: Environmental*, 2014, 146, 162-168.
6. Q. Wang, S. Tian, J. Long and P. Ning, *Catal. Today*, 2014, 224, 41-48.
7. E. Forgacs, T. Cserháti and G. Oros, *Environ. Int.*, 2004, 30, 953-971.
8. T. Robinson, G. McMullan, R. Marchant and P. Nigam, *Bioresour. Technol.*, 2001, 77, 247-255.
9. K. Li, X. Luo, X. Lin, F. Qi and P. Wu, *J. Mol. Catal. A: Chem.*, 2014, 383–384, 1-9.
10. E. S. Baeissa, *J. Alloys Compd.*, 2014, 590, 303-308.
11. U. Iriarte-Velasco, N. Chimeno-Alanís, M. P. González-Marcos and J. I. Álvarez-Uriarte, *J. Chem. Eng. Data*, 2011, 56, 2100-2109.
12. M. T. Yagub, T. K. Sen, S. Afroze and H. M. Ang, *Adv. Colloid Interface Sci.*
13. G. Z. Kyzas, N. K. Lazaridis and M. Kostoglou, *Chem. Eng. Sci.*, 2012, 81, 220-230.
14. V. K. Gupta and Suhas, *Journal of Environmental Management*, 2009, 90, 2313-2342.
15. G. Kyzas and M. Kostoglou, *Materials*, 2014, 7, 333-364.
16. M. J. Martin, A. Artola, M. D. Balaguer and M. Rigola, *Chem. Eng. J.*, 2003, 94, 231-239.
17. K. Suresh Kumar Reddy, A. Al Shoaibi and C. Srinivasakannan, *Environ. Technol.*, 2013, 35, 18-26.

18. G. Mezohegyi, F. P. van der Zee, J. Font, A. Fortuny and A. Fabregat, *Journal of Environmental Management*, 2012, 102, 148-164.
19. A. Demirbas, *J. Hazard. Mater.*, 2009, 167, 1-9.
20. P. J. M. Carrott, M. M. L. R. Carrott and R. A. Roberts, *Colloids Surf.*, 1991, 58, 385-400.
21. N. Kannan and M. M. Sundaram, *Dyes Pigm.*, 2001, 51, 25-40.
22. J. Yener, T. Kopac, G. Dogu and T. Dogu, *Chem. Eng. J.*, 2008, 144, 400-406.
23. Y. Yao, F. Xu, M. Chen, Z. Xu and Z. Zhu, *Bioresour. Technol.*, 2010, 101, 3040-3046.
24. M. A. Rauf and S. Salman Ashraf, *Chem. Eng. J.*, 2012, 209, 520-530.
25. V. C. Srivastava, I. D. Mall and I. M. Mishra, *Chem. Eng. J.*, 2007, 132, 267-278.
26. D. Li, J. Huang and R. B. Kaner, *Acc. Chem. Res.*, 2008, 42, 135-145.
27. D. Passeri, A. Biagioni, M. Rossi, E. Tamburri and M. L. Terranova, *Eur. Polym. J.*, 2013, 49, 991-998.
28. Y. Gao, Z.-H. Kang, X. Li, X.-J. Cui and J. Gong, *CrystEngComm*, 2011, 13, 3370-3372.
29. Q. M. Jia, J. B. Li, L. F. Wang, J. W. Zhu and M. Zheng, *Materials Science and Engineering: A*, 2007, 448, 356-360.
30. J. Wang, J. Wang, Z. Yang, Z. Wang, F. Zhang and S. Wang, *React. Funct. Polym.*, 2008, 68, 1435-1440.
31. G. Ćirić-Marjanović, *Synth. Met.*, 2013, 177, 1-47.
32. M. M. Ostwal, B. Qi, J. Pellegrino, A. G. Fadeev, I. D. Norris, T. T. Tsotsis, M. Sahimi and B. R. Mattes, *Ind. Eng. Chem. Res.*, 2006, 45, 6021-6031.
33. J. Wang, L. Xu, C. Cheng, Y. Meng and A. Li, *Chem. Eng. J.*, 2012, 193–194, 31-38.
34. Y. Zheng, Y. Liu and A. Wang, *Ind. Eng. Chem. Res.*, 2012, 51, 10079-10087.
35. M. A. Salem, *React. Funct. Polym.*, 2010, 70, 707-714.
36. M. M. Ayad, A. Abu El-Nasr and J. Stejskal, *Journal of Industrial and Engineering Chemistry*, 2012, 18, 1964-1969.
37. M. Ayad and S. Zaghlol, *Chem. Eng. J.*, 2012, 204–206, 79-86.
38. A. N. Chowdhury, S. R. Jesmeen and M. M. Hossain, *Polym. Adv. Technol.*, 2004, 15, 633-638.
39. M. Ayad, G. El-Hefnawy and S. Zaghlol, *Chem. Eng. J.*, 2013, 217, 460-465.
40. I. Langmuir, *J. Am. Chem. Soc.*, 1918, 40, 1361-1402.
41. H. M. F. Freundlich, *J. Phys. Chem.*, 1906, 57A, 385-470.
42. R. Sips, *J. Chem. Phys.*, 1948, 16, 490-495.
43. S. Lagergren, *K. Sven. Vetenskapsakad. Handl.*, 1898, 24, 1-39.
44. Y. S. Ho and G. McKay, *Process Saf. Environ. Prot.*, 1998, 76, 183-191.
45. M. Trchová and J. Stejskal, *Pure Appl. Chem.*, 2011, 83, 1803-1817.
46. S. Kaplan, E. M. Conwell, A. F. Richter and A. G. MacDiarmid, *J. Am. Chem. Soc.*, 1988, 110, 7647-7651.
47. E. T. Kang, K. G. Neoh and K. L. Tan, *Prog. Polym. Sci.*, 1998, 23, 277-324.
48. M. Trchová, I. Šeděnková, E. N. Konyushenko, J. Stejskal, P. Holler and G. Ćirić-Marjanović, *J. Phys. Chem. B.*, 2006, 110, 9461-9468.
49. E. C. Venancio, P.-C. Wang and A. G. MacDiarmid, *Synth. Met.*, 2006, 156, 357-369.

50. X. Wang, T. Sun, C. Wang, C. Wang, W. Zhang and Y. Wei, *Macromol. Chem. Physic.*, 2010, 211, 1814-1819.
51. W. Luzny and M. Sniechowski, *Fibres Text East Eur*, 2003, 11, 75-79.
52. C. Su, G. Wang, F. Huang and X. Li, *J. Mater. Sci.*, 2008, 43, 197-202.
53. C. Dhand, M. Das, G. Sumana, A. K. Srivastava, M. K. Pandey, C. G. Kim, M. Datta and B. D. Malhotra, *Nanoscale*, 2010, 2, 747-754.
54. A. R. Hopkins, R. A. Lipeles and S.-J. Hwang, *Synth. Met.*, 2008, 158, 594-601.
55. D. K. Bandgar, G. D. Khuspe, R. C. Pawar, C. S. Lee and V. B. Patil, *Appl Nanosci*, 2014, 4, 27-36.
56. I. Arafa, H. El-Ghanem and K. Bani-Doumi, *J. Inorg. Organomet. Polym. Mater.*, 2013, 23, 365-372.
57. G. D. Khuspe, S. T. Navale, D. K. Bandgar, R. D. Sakhare, M. A. Chougule and V. B. Patil, *Electron. Mater. Lett.*, 2014, 10, 191-197.
58. R. S. Biscaro, M. C. Rezende and R. Faez, *Polym. Adv. Technol.*, 2009, 20, 28-34.
59. T. Thanpitcha, A. Sirivat, A. Jamieson and R. Rujiravanit, *J Nanopart Res*, 2009, 11, 1167-1177.
60. L.-M. Huang, W.-R. Tang and T.-C. Wen, *J. Power Sources*, 2007, 164, 519-526.
61. G. Zhang and F. Yang, *Phys. Chem. Chem. Phys.*, 2011, 13, 3291-3302.
62. Z. D. Zujovic, M. Gizdavic-Nikolaidis and G. A. Bowmaker, *Chem. N.Z.*, 2013, 77, 87-91.
63. F. Gu, X. Yin, H. Yu, P. Wang, and L. Tong, *Opt. Express*, 2009, 17(13), 11230-11235.
64. M. Grigoras and L. Stafie, *Supramol. Chem*. 2010, 22(4), 237-248, and references cited therein.

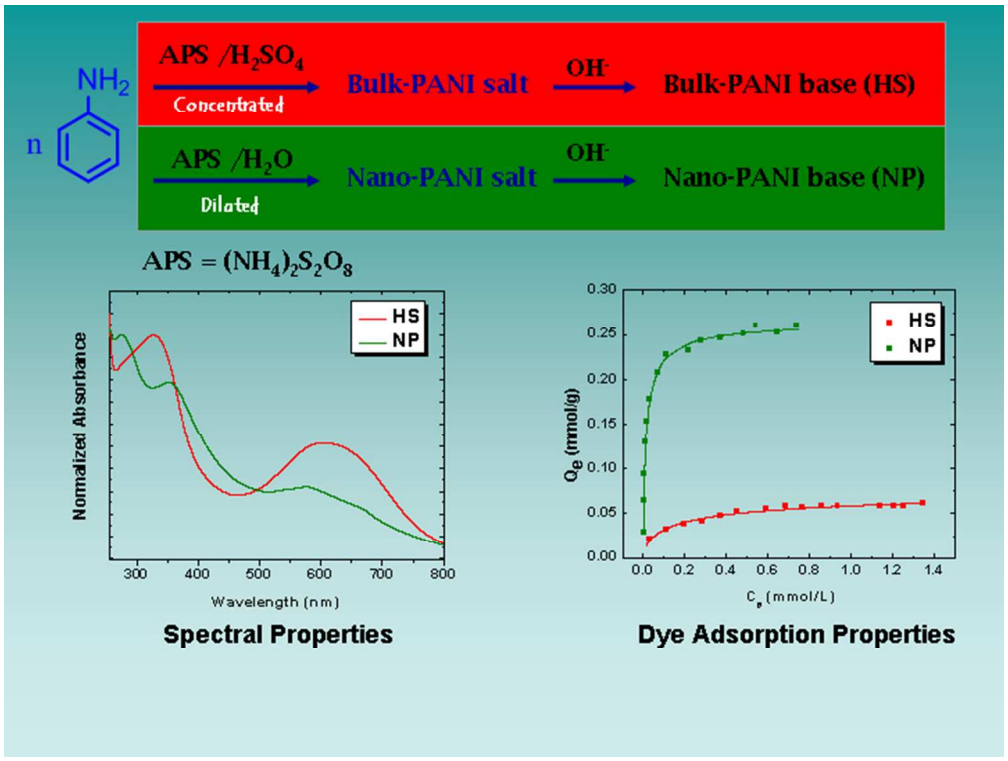

60x45mm (300 x 300 DPI)